ACS OMEGA

Open Access



http://pubs.acs.org/journal/acsodf

Article

# High-Performance Li-Organic Batteries Based on Conjugated and Nonconjugated Schiff-Base Polymer Anode Materials

Jinkai Zhang, Xiaoyue Mu,* and Ying Mu*

Cite This: *ACS Omega* 2024, 9, 12967−12975

Read Online

ACCESS | Metrics & More | Article Recommendations | Supporting Information

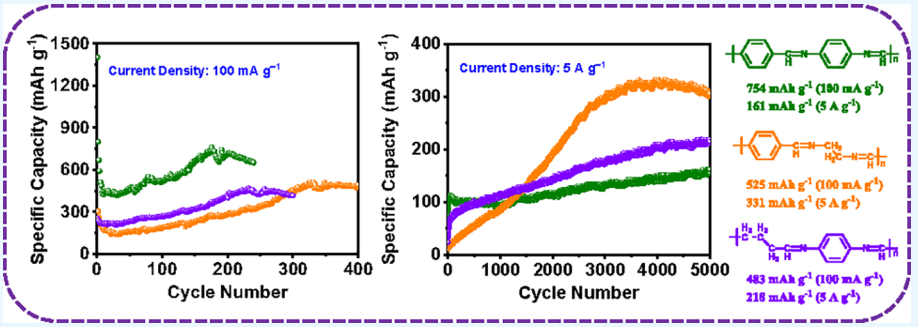


**ABSTRACT:** In recent years, organic materials have been increasingly studied as anode materials in lithium-ion batteries (LIBs) due to their remarkable advantages, including abundant raw materials, low prices, diverse structures, and high theoretical capacity. In this paper, three types of aromatic Schiff-base polymer materials have been synthesized and examined as anode materials in LIBs. Among them, the polymer $[C_6H_4N = CHC_6H_4CH{=}N]_n$ (TTD-PDA) has a continuous conjugated backbone (label as conjugated polymer), while polymers $[(CH_2)_2N{=}CHC_6H_4CH{=}N]_n$ (TTD-EDA) and $[C_6H_4N{=}CH(CH_2)_3CH{=}N]_n$ (GA-PDA) have discontinuous conjugated back-bones (label as nonconjugated polymer). The organic anodes based on TTD-PDA, TTD-EDA, and GA-PDA for LIBs are discovered to represent high reversible specific capacities of 651, 492, and 416 mAh $g^{-1}$ at a current density of 100 mA $g^{-1}$ as well as satisfactory rate capabilities with high capacities of 210, 90, and 178 mAh $g^{-1}$ and 105, 57, and 122 mAh $g^{-1}$ at current densities of 2 and 10 A $g^{-1}$, indicating that these Schiff-base polymers are all promising anode materials for LIBs, which broadens the design of organic anode materials with high specific capacity, superior rate performance, and stable cycling stability.

## 1. INTRODUCTION

With the increasingly severe energy crisis and environmental issues, the establishment of a clean and renewable energy system has become an important task for the scientific community.[1] Natural sources of solar, tidal, and wind power, though clean and renewable, are not sustainable. Energy storage equipment can be developed to store energy or substances in nature and then convert it into electric energy to release when energy is needed, thus achieving sustainable energy supply.[2] Rechargeable batteries are energy storage devices that convert chemical energy to electric energy by redox reaction. Among them, lithium-ion batteries (LIBs) are the most widely used secondary batteries. LIBs have many advantages, such as high energy density, long cycle life, low self-discharge rate, and no memory effect, and their performance is much higher than that of nickel−chromium, lead-acid, and other secondary batteries. With these advantages, LIBs are widely used in mobile phones, laptops, electric cars and other electrical devices.[3,4]

As the market grows larger and expands into more and more high-end power applications, such as orbiting satellites and deep space exploration, LIBs must be of higher quality. Electrode materials are an important index to improve the performance of LIBs.[5,6] The traditional electrode materials for LIBs are mostly inorganic materials such as carbon materials commonly used in the anode and metal oxides commonly used in the cathode. The theoretical specific capacity of these inorganic electrode materials is low, and the degradation of the material will lead to the reduction of battery life after a long time cycling.[7−10] In comparison, organic electrode materials have the advantages of high theoretical specific capacity, designable structure, low price, and environmental friendliness.[11−14] Because of these advantages, organic electrode materials have attracted more and more attention as a new kind of electrode materials.[15,16]

Schiff base materials as organic electrode materials have been studied more and more. Since polymers are insoluble in

Received: November 21, 2023
Revised: February 15, 2024
Accepted: February 21, 2024
Published: March 7, 2024

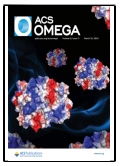

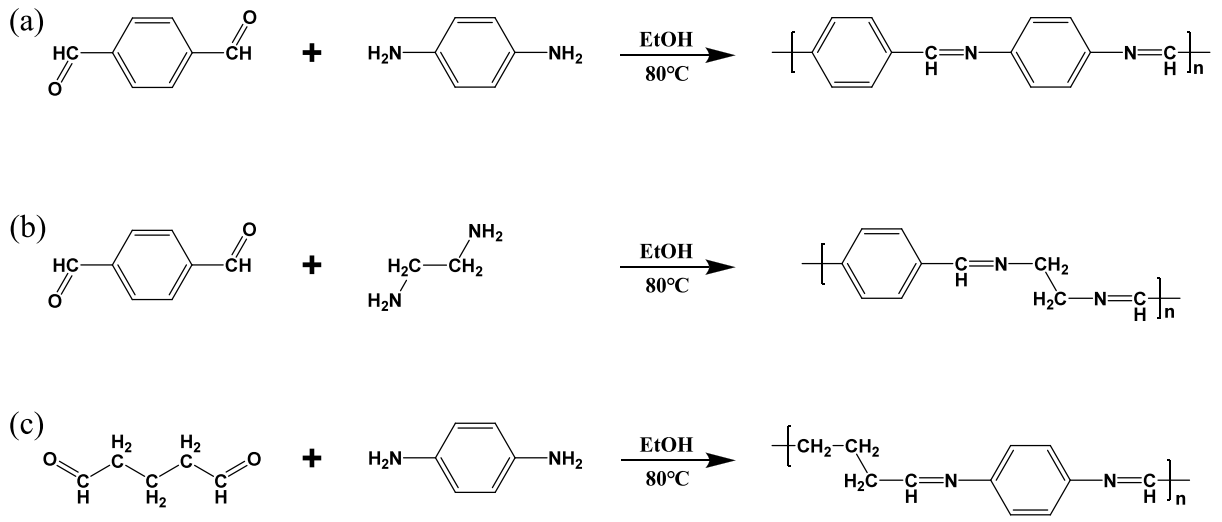


**Figure 1.** (a) Synthesis of conjugated Schiff-base TTD-PDA; (b) synthesis of nonconjugated Schiff-base TTD-EDA; (c) synthesis of nonconjugated Schiff-base GA-PDA.

most organic solvents, Schiff base materials used for electrode materials are usually Schiff base polymers to avoid the electrode materials dissolving into the electrolyte.[17−20] Traditional Schiff base polymer electrode materials are usually large conjugated systems because conjugated systems are more conducive to electron transfer. To study the lithium storage properties of different Schiff base polymers, three kinds of Schiff base polymers with similar structures were prepared in the experiment in this work, one of which was conjugated Schiff base polymer and the other two were unconjugated Schiff base polymer. These Schiff base materials TTD-PDA, TTD-EDA, and GA-PDA were prepared by a simple ketoamine condensation reaction using terephthalaldehyde (TTD) and *p*-phenylenediamine (PDA), TTD and ethylenediamine (EDA), glutaraldehyde solution 50% (GA), and PDA as raw materials (Figure 1). When they are used as anode materials for LIBs, they all exhibit excellent electrochemical properties, such as cycling performance and rate capabilities. Herein, we report the synthesis, characterization, and electrochemical properties of these materials in detail and discuss the property differences due to their different structures.

## 2. EXPERIMENTAL SECTION

**2.1. Materials Synthesis.** *2.1.1. Preparation of the TTD-PDA.* A 100 mL round-bottom flask is charged with terephthalaldehyde (TTD) (1.34 g, 10 mmol), *p*-phenylenediamine (PDA) (1.08 g, 10 mmol), and absolute ethanol (50 mL). The mixture was heated to 80 °C, stirred, and refluxed for 3 days. After cooling of the mixture obtained from the reaction to room temperature (25 °C), orange precipitates can be observed. By filtering of the orange precipitates, the orange solids were collected, and the filtrate was repeatedly cleaned with ethanol and tetrahydrofuran (THF) until it was colorless. The final product TTD-PDA (1.96 g, 95%) was produced as an orange powder after drying the orange solid refined in a 70 °C vacuum oven for 12 h.

*2.1.2. Preparation of the TTD-EDA.* A 100 mL round-bottom flask is charged with TTD (1.34 g, 10 mmol), ethylenediamine (EDA) (0.60 g, 10 mmol), and absolute ethanol (50 mL). The mixture was heated to 80 °C, stirring and reflux for 3 days. After the mixture obtained from the reaction was cooled to room temperature (25 °C), faint yellow precipitates could be observed. By filtering the faint yellow precipitates, the buff solids were collected, and the filtrate was repeatedly cleaned with ethanol and tetrahydrofuran (THF) until it was colorless. The final product TTD-EDA (1.42 g, 90%) was produced as pale yellow powder after drying the buff solid refined in a 70 °C vacuum oven for 12 h.

*2.1.3. Preparation of the GA-PDA.* A 100 mL round-bottom flask is charged with glutaraldehyde solution 50% (GA) (2.00 g, 10 mmol), PDA (1.08 g, 10 mmol), and absolute ethanol (50 mL). The mixture was heated to 80 °C, stirring and reflux for 3 days. After cooling of the mixture obtained from the reaction to room temperature (25 °C), brown precipitates can be observed. By filtering of the dark precipitates, the brown solids were collected, and the filtrate was repeatedly cleaned with ethanol and tetrahydrofuran (THF) until it was colorless. The final product GA-PDA (1.51 g, 88%) was synthesized as a brown powder after drying the brown solid refined in a 70 °C vacuum oven for 12 h.

**2.2. Material Characterizations.** For the purpose of characterizing the TTD-PDA, TTD-EDA, and GA-PDA, a variety of spectroscopic and analytical methods were used, including Fourier transform infrared spectroscopy (FT-IR), elemental analysis (EA), powder X-ray diffraction analysis (PXRD), thermogravimetric analysis (TGA), and field emission scanning electron microscopy (FESEM). The FT-IR spectra were examined using KBr pellets in the wavenumber range of 4000−450 $cm^{-1}$ by a Nicolet is5 spectrometer (Thermo Fisher, America). EA of organic molecules was conducted on the element analyzer (Elementar Vario EL cube, Elementar, Germany). The crystallinity of organic molecules was collected on powder X-ray diffraction (PXRD) measurements (PANalytical B.V., Empyrean, Netherlands) with a Cu K$\alpha$ radiation range of 5 to 90°. Morphological characterization of organic samples was observed through field emission scanning electron microscopy (SU8020, HITACHI, Japan). Thermogravimetric analysis (TGA) was conducted on a thermogravimetric analyzer (STA449F3-QMS403D, Germany) with a temperature range of 40 to 800 °C at a heating rate of 10 °C $min^{-1}$ under a $N_2$ atmosphere.

**2.3. Electrochemical Measurement.** The active materials (TTD-PDA, TTD-EDA and GA-PDA), conductive carbon nanotubes, and poly(vinylidene fluoride) (PVDF) were


https://doi.org/10.1021/acsomega.3c09299
ACS Omega 2024, 9, 12967−12975

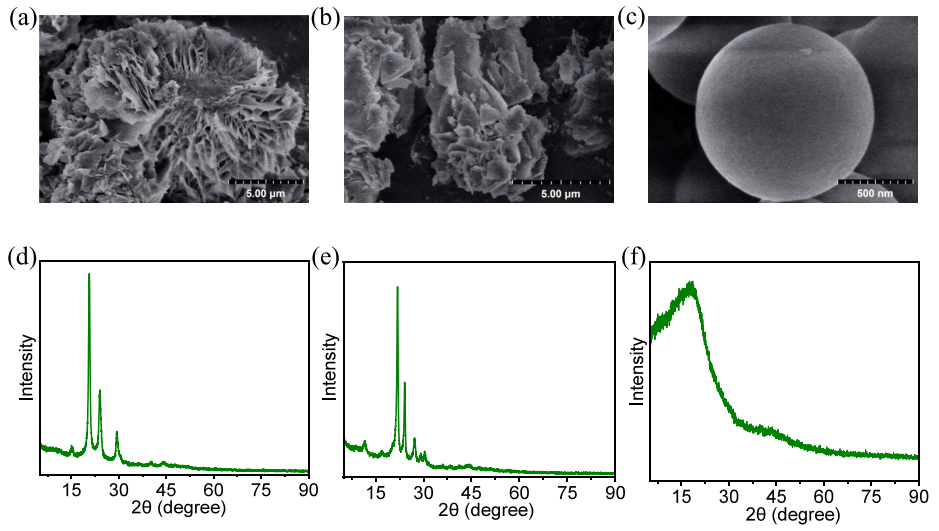


**Figure 2.** SEM images of (a) TTD-PDA, (b) TTD-EDA, and (c) GA-PDA; XRD patterns of (d) TTD-PDA, (e) TTD-EDA, and (f) GA-PDA.

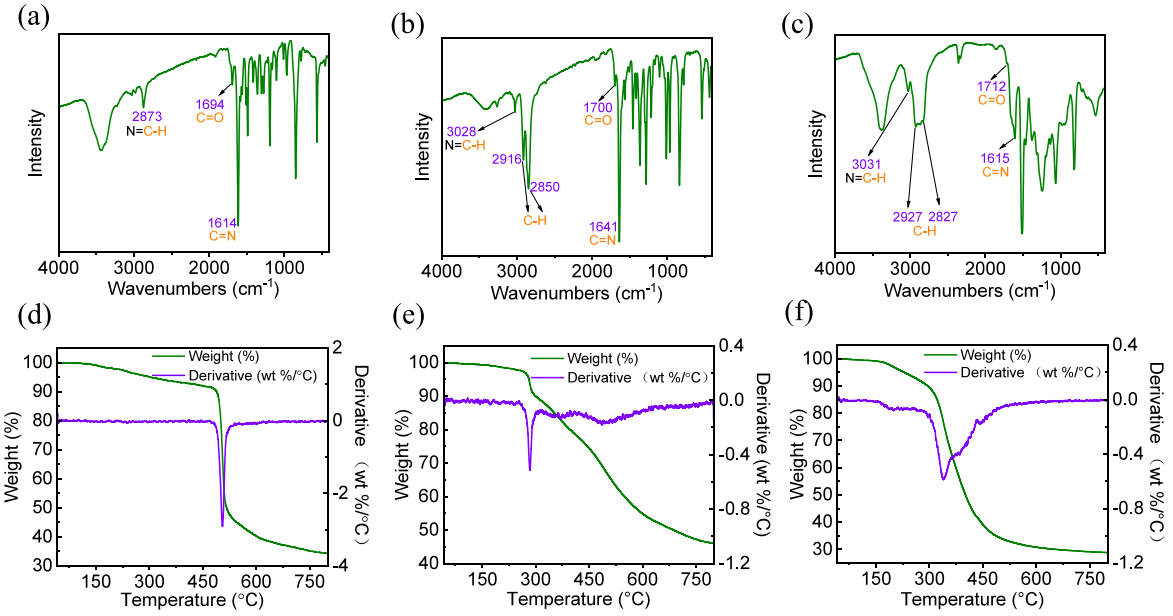


**Figure 3.** FT-IR spectra of (a) TTD-PDA, (b) TTD-EDA, and (c) GA-PDA; TGA/dTGA curves of the (d) TTD-PDA, (e) TTD-EDA, and (f) GA-PDA compounds in a $N_2$ atmosphere.

combined in a weight ratio of 5:4:1 to create the electrode slurries. *N*-Methyl-2-pyrrolidinone (NMP) served as the dispersant. Following that, the resulting slurry was coated on a piece of copper foil and dried under vacuum for 12 h at 60 °C. Lithium metal served as the counter electrode, commercially available polypropylene film served as the separator, and the electrolyte solution was composed of 1 M $LiPF_6$ dissolved in ethylene carbonate (EC)/dimethyl carbonate (DMC) (1:1 by volume) with 5% fluoroethylene carbonate (FEC). Half-cells were packaged in CR2016 coin-type cells. The coin-type cells were assembled in a glovebox that was filled with argon ($H_2O$ < 1 ppm, $O_2$ < 1 ppm). Galvanostatic charge−discharge tests, rate capacities at various current densities, cyclic voltammetry (CV) measurements, and electrochemical impedance spectroscopy (EIS) measurements were used to evaluate the built CR2016 coin-type cells. Using CT2001A battery test equipment (LANHE, China), tests of galvanostatic charge−discharge and rate capacities at various current densities were made in the voltage range of 0.02−3 V vs $Li/Li^+$. At a scanning rate of 0.2 mV $s^{-1}$, CV measurements were performed on the VersaSTAT 3 electrochemical working station (America) in the voltage range of 0.02−3.0 V. Using a CHI760E electrochemical workstation (China) with a frequency range of 0.01 Hz to 100 kHz, EIS measurements were performed.

## 3. RESULTS AND DISCUSSION

### 3.1. Morphological and Structural Characterization.

The morphology of the Schiff-base polymers TTD-PDA, TTD-EDA, and GA-PDA were explored by SEM. As shown in Figure 2a, the TTD-PDA exists a petal shape with a porous structure, which is about 15 $\mu$m in diameter. The morphology of TTD-EDA is shown in Figure 2b. It is an irregular flake with a long diameter of about 10 $\mu$m and a short diameter of about 5 $\mu$m. GA-PDA shows spherical particles with diameters of about 800 nm (Figure 2c). Figure 2d−f shows the XRD pattern of these



https://doi.org/10.1021/acsomega.3c09299
ACS Omega 2024, 9, 12967−12975

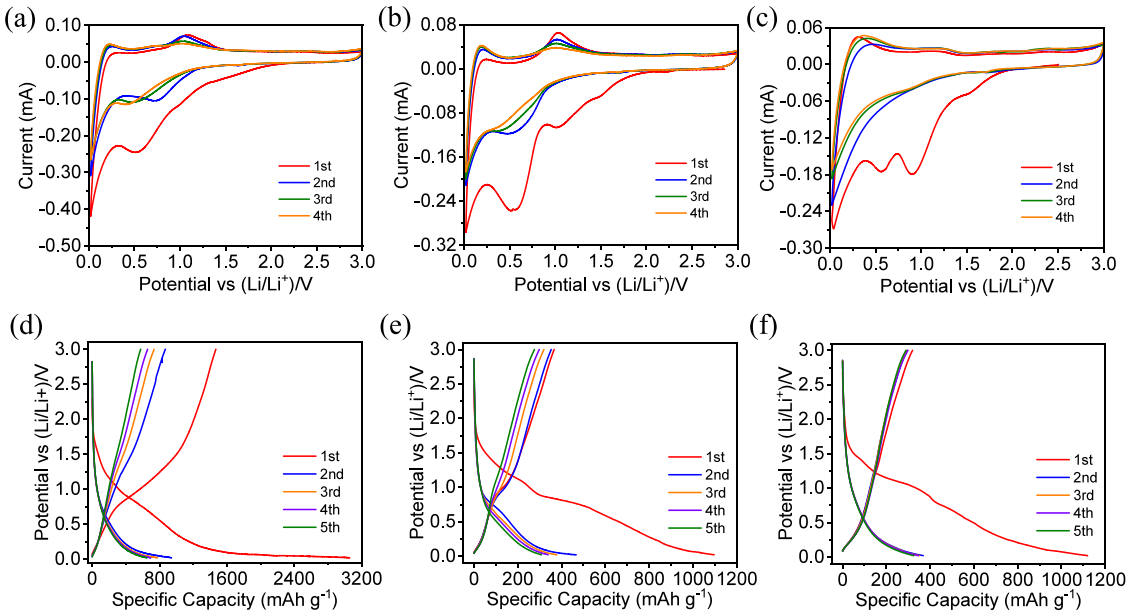


**Figure 4.** CV curves of the primary four cycles of (a) TTD-PDA, (b) TTD-EDA, and (c) GA-PDA; charge−discharge curves for the initial five cycles of (d) TTD-PDA, (e) TTD-EDA, and (f) GA-PDA.

three Schiff base polymers. From Figure 2d,e, it can be seen that there are multiple strong diffraction peaks between 15 and 30°, which indicates that both TTD-PDA and TTD-EDA have very good crystallinity. XRD pattern of GA-PDA is shown in Figure 2f, only one small broad peak around 18° was observed, suggesting the weak crystallinity of the GA-PDA material.

The FT-IR revealed the chemical structure of the Schiff-base polymers TTD-PDA, TTD-EDA and GA-PDA in Figure 3a−c. As ascribed, all three Schiff-base polymers showed the main characteristic peak of the imine group. In the FT-IR spectra, the peaks at 1614, 1641, and 1615 $cm^{-1}$ correspond to stretching vibrations of C═N bonds of these three polymers respectively, which are evidence of imines being synthesized by the reaction. Besides, the small absorption peaks observed at 1694, 1700, and 1712 $cm^{-1}$ are assigned to the stretching vibration of C═O bonds in the terminal aldehyde groups of TTD-PDA, TTD-EDA, and GA-PDA. Furthermore, in the spectrum of TTD-EDA, two peaks at 2850 and 2916 $cm^{-1}$ correspond to the stretching vibrations of C−H, and the peak at 3028 $cm^{-1}$ should be the stretching vibrations of unsaturated C−H bonds (Figure 3b). As for the spectrum of GA-PDA, the bands located between 2827 and 2927 $cm^{-1}$ could be attributed to the stretching vibrations of C−H. Compared with TTD-EDA, there are more saturated C−H bonds in GA-PDA, so the absorption peaks in the spectrum are more complex. Similar to TTD-EDA, the peak at 3031 $cm^{-1}$ is assigned to the stretching vibrations of unsaturated C−H bonds (Figure 3c). In addition, as can be seen from the spectrum of TTD-PDA, there are no saturated C−H bonds in TTD-PDA, which is consistent with our expected result. Also, it is worth mentioning that the position of absorption peak of unsaturated C−H bond in TTD-PDA showed obvious blueshift (2873 $cm^{-1}$) compared with the other two substances, which was probably caused by the adjacent benzene rings that have an electron donating conjugation effect[33−36] (Figure 3a). All of these results indicated that the TTD-PDA, TTD-EDA, and GA-PDA were successfully prepared. The elemental analysis findings for TTD-PDA (C: 80.5%, H: 4.9%, N: 14.6%), TTD-EDA (C: 76.3%, H: 6.4%, N: 17.3%), and GA-PDA (C: 77.3%, H: 7.0%, N: 15.7%) are extremely close to the theoretical values, indicating that these materials were successfully prepared.

**3.2. Thermal Stabilities of Schiff-Base Polymers.** Thermogravimetric analysis was utilized to study the thermal stabilities of the Schiff-base polymers. The testing temperature range is between 40 and 800 °C. The thermogravimetric (TG) and derivative thermogravimetric (DTG) curves in nitrogen atmosphere are revealed in Figure 3d−f. As illustrated in Figure 3d, it can be seen from the DTG curve that the derivative curve begins to decrease significantly from around 480 °C. Combined with the TG curve, the weight curve has an approximate vertical decline at this temperature. This indicates that the thermal decomposition temperature of TTD-PDA is around 480 °C. The same analysis method can be used to obtain the thermal decomposition temperature of TTD-EDA at about 270 °C (Figure 3e). Unlike the above two polymers, the DTG curve of GA-PDA shows that a large band in the derivative curve is preceded by a smaller band. Combined with the TG curve, it can be seen that when the temperature is around 175 °C, the weight curve first shows a small slope decline, and when the temperature reaches around 300 °C, the weight curve begins to drop sharply (Figure 3f). This indicates that partial degradation of the material occurred near 175 °C, possibly due to the breakage of the longer carbon chain of the glutaraldehyde matrix at that temperature. At about 300 °C, complete decomposition of the material occurs. The above conclusions show that the thermal decomposition temperature of these three materials is relatively high, much higher than the operating temperature of lithium-ion batteries. Therefore, from the point of view of thermal stability, the prepared TTD-PDA, TTD-EDA, and GA-PDA polymer materials can be utilized as superior electrode materials.

**3.3. Electrochemical Behaviors and Battery Performance.** Electrochemical behaviors of the TTD-PDA as well as the TTD-EDA and GA-PDA were evaluated by cyclic voltammetry measurements with a scan rate of 0.2 mV $s^{-1}$ in


https://doi.org/10.1021/acsomega.3c09299
ACS Omega 2024, 9, 12967−12975

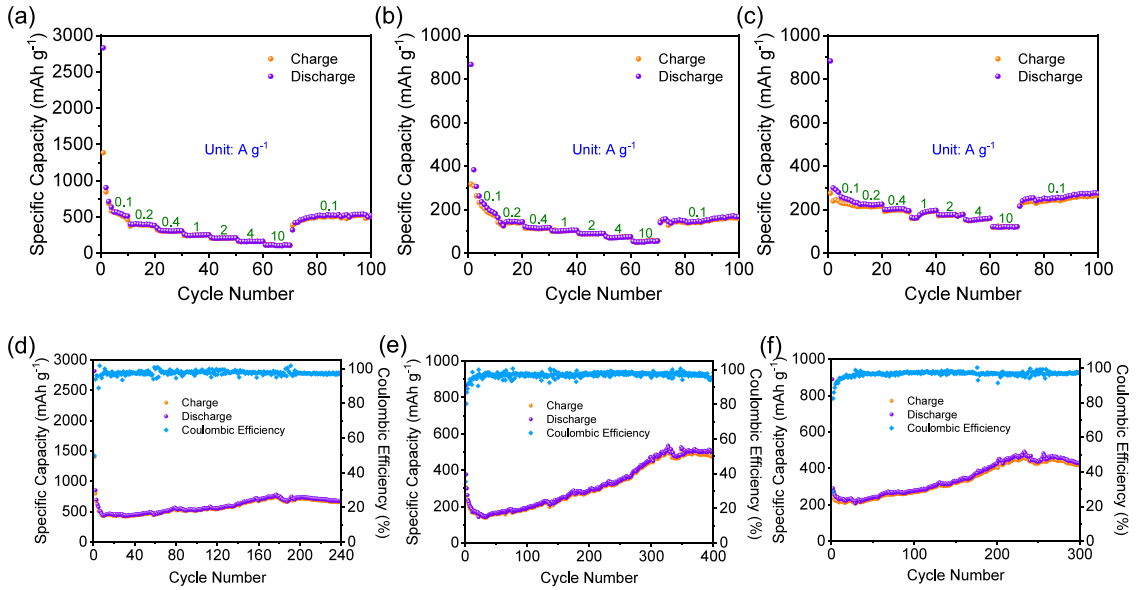


**Figure 5.** Actual rate performance of the Schiff-base electrodes (a) TTD-PDA, (b) TTD-EDA, and (c) GA-PDA and the actual cycle stability of the Schiff-base electrodes (d) TTD-PDA, (e) TTD-EDA, and (f) GA-PDA at a current of 100 mA $g^{-1}$.

the potential ranging from 0.02 to 3 V and exhibited in Figure 4a−c. All three Schiff-bases showed the weak and irreversible reduction peaks at about 1.5 V in the first negative scan, which can be explained to the formation of a stable solid electrolyte interface (SEI) in the first cycle.[21,22,28,40] In addition, the three polymers indicated similar redox potentials at the initial scan. They all present three reduction peaks near 1.0 V, around 0.6 V, and below 0.3 V corresponding to the typical lithium enolization reaction of terminal carbonyl group, the insertion of lithium ions on the C═N bond,[23] and the gradual intercalation of lithium ions into the unsaturated C═C in the benzene ring, respectively.[24,25] Certainly, each reduction peak may correspond to one or more electrochemical reactions. The oxidation peaks of the three substances in the first positive scan are located around 0.25 and 1.1 V, which may correspond to the regeneration of C═C and C═N after delithiation. From the second scan, all three materials exhibited reduction peaks different from those of the initial scan. The new reduction peak of TTD-PDA appeared close to 0.8 V and moved to around 0.4 V after the fourth cycle. The new reduction peaks of TTD-EDA and GA-PDA appeared near 0.7 and 0.9 V, respectively. These reduction peaks ought to be caused by lithium insertion into the C═N bond of each imine groups.[28,29] It is worth mentioning that, from the weakening of the oxidation peak near 1.1 V and the strengthening of the oxidation peak near 0.25 V, it can be concluded that the electrochemical activity of C═N in the three polymers is becoming weaker, while the electroactive activity of C═C belonging to the benzene ring framework is continuously strengthening with the number of cycles increasing. Moreover, it can be definitely spotted from the Figure 4a−c that the reduction peak potential of C═N decreases or the peak intensity weakens. This indicates that as the charging and discharging continue, the $Li^+$ inserting into C═N becomes more and more difficult. These results illustrate that the electrochemical activity of imine groups may not be fully utilized in linear Schiff-base structures.[40]

The charge−discharge profiles of polymer electrodes at 0.1 A $g^{-1}$ in the potential range 0.02−3 V are shown in Figure 4d−f. No evident potential plateaus are detected in the charge−discharge curves of any of the three anode materials, indicating the possible multiple $Li^+$ storage processes.[26,39] In the first cycle, it can be seen that all three materials have a distinct slope below 0.3 V, corresponding to the lithium ion inserted into the C═C of the benzene ring. They also have a small slope near 0.6 V; only the TTD-PDA material is less noticeable, but the slope of the curve also changes, which corresponds to the lithium ion intercalated in the C═N of the imide group. These phenomena are highly consistent with the CV curves. The first apparent discharge/charge capacities of TTD-PDA, TTD-EDA, and GA-PDA are 3059/1469, 1097/367, and 1119/319 mAh $g^{-1}$. In order to exclude the contribution of carbon nanotubes to the capacity value, the first actual discharge/charge specific capacity values of TTD-PDA, TTD-EDA, and GA-PDA were calculated by applying the equation $S_s = S_{sa} - 0.8S_c$ ($S_s$: actual specific capacity of the Schiff base; $S_{sa}$: apparent specific capacity of Schiff base; $S_c$: specific capacity of CNT), which were 2817/1401, 855/299, and 877/251 mAh $g^{-1}$, corresponding to first Coulombic efficiencies (CEs) of 49.7, 35.0, and 28.6% (please refer to the Supporting Information for particular calculation methods and CNT specific capacity information). Similar to many other anode materials, SEI formation contributes to the irreversible capacity that results in comparatively low CE in the initial charge/discharge procedure. In addition, the insertion of lithium ions into certain functional groups in organic materials cannot be extracted also leads to a significant decrease in CE. Moreover, it can be seen that the specific capacity of the three anode materials shows an attenuation trend in the first five charging and discharging cycles. After the fifth cycle, the apparent and actual reversible specific capacities of TTD-PDA, TTD-EDA, and GA-PDA are 575/509, 276/210, and 290/224 mAh $g^{-1}$. Among them, TTD-PDA has the highest actual reversible specific capacity, approximately 1.4 times that of the theoretical capacity of graphite anode. The actual reversible specific capacity of TTD-EDA is the lowest, about 56% than the theoretical capacity of graphite anode.


https://doi.org/10.1021/acsomega.3c09299
ACS Omega 2024, 9, 12967−12975

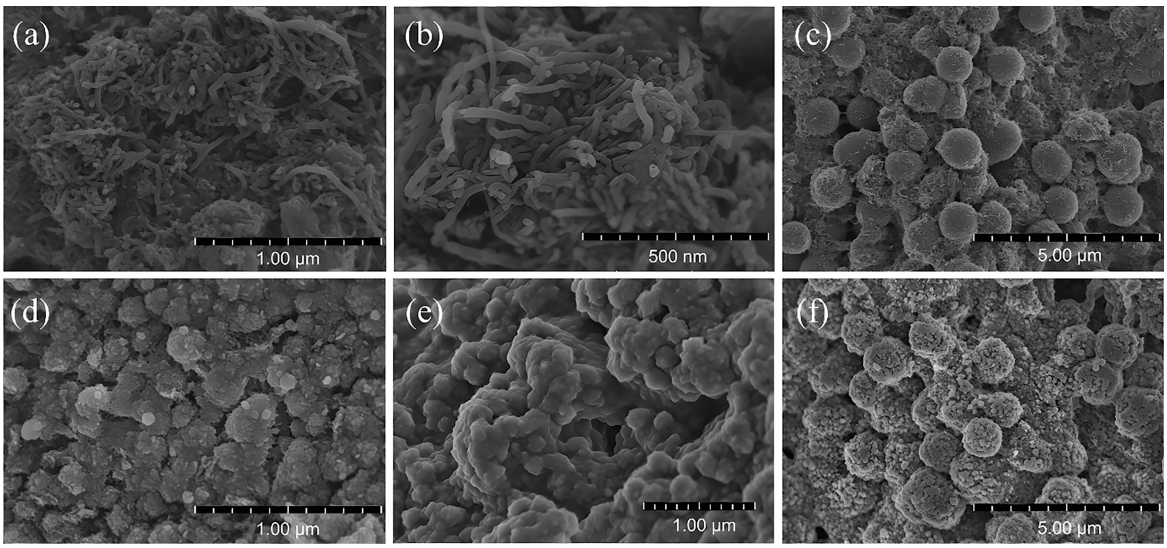


**Figure 6.** SEM images of the polymer electrodes: (a) TTD-PDA, (b) TTD-EDA, and (c) GA-PDA before the cycle; (d) TTD-PDA, (e) TTD-EDA, and (f) GA-PDA after 100 cycles.

The TTD-PDA, TTD-EDA, and GA-PDA electrodes are discharged−charged at various current densities ranging from 0.1 to 10 A $g^{-1}$, as depicted in Figure 5a−c. As the current density steadily raises, the profiles of the three anodes maintain stability for up to 10 cycles at each rate. The actual charging specific capacities of the TTD-PDA, TTD-EDA, and GA-PDA electrodes are 460, 375, 302, 253, 210, 162, 105 mAh $g^{-1}$, 171, 141, 115, 104, 90, 76, 57 mAh $g^{-1}$, and 219, 216, 200, 192, 178, 160, 122 mAh $g^{-1}$ at the current densities of 0.1, 0.2, 0.4, 1, 2, 4, and 10 A $g^{-1}$, respectively. When the current density is reset to 0.1 A $g^{-1}$, the reversible capacities of these anodes still retain 422, 156, and 240 mAh $g^{-1}$ with nearly inappreciable capacity fading, indicating that these anodes exhibit remarkable stabilization during rapid charging and discharging processes. Furthermore, the specific capacity of them also stays steady during the subsequent 30 cycles, and the CE of 90% or above is present for each charge and discharge, further demonstrating the exceptional stability, excellent rate performance, and outstanding reversibility of these electrodes. It is worth mentioning that although the specific capacity of GA-PDA is only half that of TTD-PDA at a current density of 0.1 A $g^{-1}$, the specific capacity of GA-PDA evaporates very slowly as the current density gradually increases. When the current density increases to 4 A $g^{-1}$, the specific capacity of GA-PDA is almost equivalent to that of TTD-PDA. When the current density reaches 10 A $g^{-1}$, the specific capacity of GA-PDA exceeds that of TTD-PDA. This indicates that GA-PDA prefers rate performance.

Figure 5d−f identifies the three anodes' long-term cycling stability at a modest current density of 100 mA $g^{-1}$. All Coulombic efficiencies of the three anodes are above 90% after the fifth cycle, exhibiting remarkable cyclic stability. In addition, different from traditional LIBs, the specific capacities of these electrodes present an apparent increasing trend after 30 cycles. After 240, 400, and 300 times of charging and discharging, the actual charging specific capacities of TTD-PDA, TTD-EDA, and GA-PDA reached 651, 492, and 416 mAh $g^{-1}$, which are 1.5, 3.5, and 2 times of their 30th charge specific capacity, respectively. The existence of irreversible electrochemical processes and the low conductivity of the materials might be the cause of the specific capacity decline observed during the first 30 cycles.[41] The electrochemically active groups in the compounds, such as benzene rings, will be continuously activated as the charging and discharging process proceeds. This will enable the electrode to insert more lithium ions, which is consistent with the discussion in the previous section of cyclic voltammetry, thus significantly increase the specific capacity of the anodes.[37,38] In addition, through data comparison, it can be intuitively seen that the anode material of the nonconjugated system has a larger proportion of capacity improvement after cycling, which may be due to the fact that the electrochemical active groups in the nonconjugated structure are initially in a suppressed state. This indicates that organic nonconjugated materials are a class of potential electrode materials. It can exhibit excellent electrochemical properties after activation.

The possible Li storage mechanism of the Schiff-base electrodes was discussed. Based on the equation $C_{thro} = nF/(3.6M)$, in which $C_{thro}$ is the theoretical specific capacity, $n$ is the number of electrons per repeating unit participated in the redox reaction, $F$ is the Faraday constant, and $M$ means the molecular weight of repeating unit. The $M$ values of TTD-PDA, TTD-EDA, and GA-PDA are 206, 158, and 172, respectively. The maximum actual charging capacities of TTD-PDA, TTD-EDA, and GA-PDA in the complete cycle are 754, 525, and 483 mAh $g^{-1}$, respectively. According to the equation, the theoretical specific capacity contributions of a $Li^+$ inserted into the electrodes of TTD-PDA, TTD-EDA, and GA-PDA are 130.1, 169.7, and 155.8 mAh $g^{-1}$, respectively, which indicates that the number of lithium ions inserted into each unit of these anodes should be 6, 4, and 4. Therefore, it is obvious that among the three electrode materials, not only the redox reaction of C═N contributes to the specific capacity but the behavior of lithium ion insertion into the benzene ring structure also contributes to a higher specific capacity.[30−32] Moreover, in the conjugated structure system, the aromatic benzene ring structure is significantly able to accommodate more lithium ions, thus providing a higher specific capacity.

The batteries of these anodes were disassembled to gain insight into the morphological change by SEM testing to make further efforts to examine the cycling behavior of the TTD-PDA, TTD-EDA, and GA-PDA electrode materials. The


https://doi.org/10.1021/acsomega.3c09299
ACS Omega 2024, 9, 12967−12975

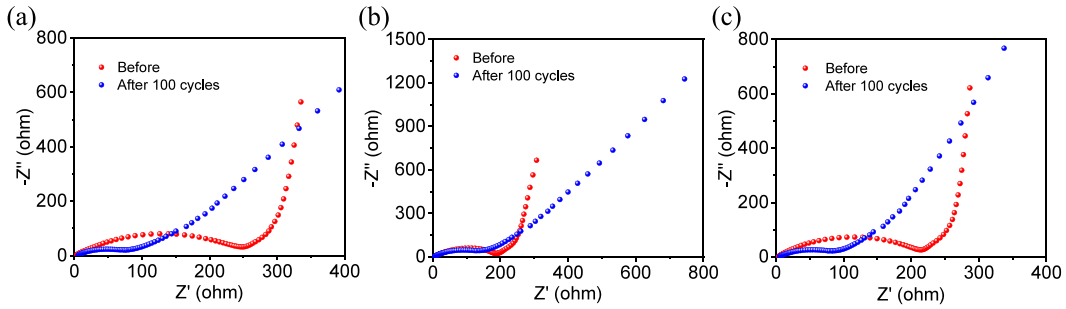


**Figure 7.** Electrochemical impedance spectra of the Schiff-base electrodes: (a) TTD-PDA, (b) TTD-EDA, and (c) GA-PDA prior to cycle and after 100 cycles.

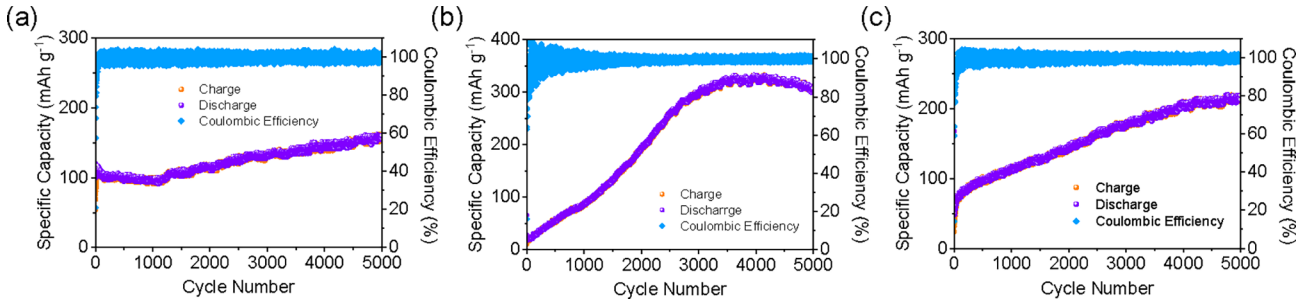


**Figure 8.** Actual long-term cycling performance of (a) TTD-PDA, (b) TTD-EDA, and (c) GA-PDA at a current density of 5 A $g^{-1}$.

results are presented in Figure 6. Figure 6a–c shows the morphology of the pristine electrodes TTD-PDA, TTD-EDA, and GA-PDA. It can be seen that the active substance is regularly dispersed in the electrode, and there is a large amount of well-distributed wrapped conductive carbon materials around it. The rate of electron transport can be accelerated by close contact between conductive carbon and active components. The morphology of the electrodes of TTD-PDA, TTD-EDA, and GA-PDA after 100 times charge–discharge is exhibited in Figure 6d–f. After an adequate charge–discharge cycle, the conductive carbon material is fully embedded into the anode materials, thus enhancing their electrical conductivity. In addition, SEM images reveal that after numerous times cycling of charge and discharge, the material itself still retains a large number of pores without pulverization and breakage. The morphological stability of TTD-PDA, TTD-EDA, and GA-PDA anodes is supposed to be a prominent factor for electrode materials with fine cyclic behavior.

The electrochemical impedance spectroscopy (EIS) was applied to comprehend the electrochemical reaction kinetics of the TTD-PDA, TTD-EDA, and GA-PDA electrodes (before cycling and after 100 cycles). Figure 7 demonstrates the Nyquist plots of the three electrodes tested in the frequency range of 100 kHz to 0.1 Hz before and after the cycle. In all three of these sets of Nyquist plots, a slope in the low frequency region and a semicircle in the high-to-medium frequency region are observed. The former indicates the Warburg impedance, which relates to the diffusion of $Li^+$ at the solid-phase interface, while the latter reflects a polarization resistance, which corresponds to the charge transfer process and electrolyte transport procedure. A minor semicircle and a shorter high-frequency intercept commonly signify more desirable interfacial charge kinetics, and the diameter of the semicircle on the $Z_{re}$ axis is capable of estimating the magnitude of charge transfer resistance ($R_{ct}$).[27] Apparently, whether before cycling or after 100 cycles, the Nyquist plots of these samples have similar configurations. Nevertheless, after 100 cycles, the semicircles and intercepts of the three Nyquist plots became significantly smaller and the $R_{ct}$ values of the three electrodes (TTD-PDA: 76.9 Ω, TTD-EDA: 136.1 Ω, GA-PDA: 79.3 Ω) are dramatically smaller than that before cycling (TTD-PDA: 250.6 Ω, TTD-EDA: 189.6 Ω, GA-PDA: 216.1 Ω), implying that the electrochemical reaction kinetics and electrode activation process were enhanced gradually. The relatively low impedance of the three anodes after 100 cycles indicates that the electrodes have low charge transfer resistance, which has a positive impact on $Li^+$ diffusion and electron transfer.

To test the specific capacity and cyclic stability of TTD-PDA, TTD-EDA and GA-PDA at high current density, the three anodes were being cycled 5,000 times at a current density of 5 A $g^{-1}$. As shown in Figure 8, the actual specific capacity of TTD-EDA is the largest of the three, after about 4,000 times repeated charges and discharges, its charging specific capacity reaches its maximum value of approximately 330 mAh $g^{-1}$. This result further demonstrates that the electrochemical active groups of nonconjugated organic polymers can be activated after repeated charge/discharge, resulting in a significant increase in specific capacity. After this, the specific capacity of TTD-EDA slightly decreased, and at the 5,000th cycle, its charging specific capacity could still reach 305 mAh $g^{-1}$. The specific capacity of GA-PDA also showed an upward trend, compared with TTD-EDA, its rising speed was relatively slow and generally stable at around 210 mAh $g^{-1}$ after 4,300 cycles. Surprisingly, the TTD-PDA with conjugate structure does not perform as well as the other two nonconjugated compounds at high current density. Its specific capacity dropped slightly in the first 1,100 cycles and then began to rise very slowly, and the final actual charge specific capacity was about 161 mAh $g^{-1}$. In general, all three Schiff-base polymers exhibit extremely high cyclic stability and satisfactory specific capacity at high


https://doi.org/10.1021/acsomega.3c09299
ACS Omega 2024, 9, 12967–12975

current densities, making them potential electrode materials for application.

## 4. CONCLUSIONS

In conclusion, we designed and successfully prepared three Schiff-base organic anodes; all three anodes exhibit excellent electrochemical properties. Regardless of whether it is a conjugated molecule, the imine structure and benzene ring skeleton can bind a large number of lithium ions. The LIBs based on these electrodes provide high reversible capacity (TTD-PDA: 651 mAh $g^{-1}$ at 0.1 A $g^{-1}$ after 240 cycles, TTD-EDA: 492 mAh $g^{-1}$ at 0.1 A $g^{-1}$ after 400 cycles, GA-PDA: 416 mAh $g^{-1}$ at 0.1 A $g^{-1}$ after 300 cycles), satisfactory rate performance (TTD-PDA: 210 mAh $g^{-1}$ at 2 A $g^{-1}$, TTD-EDA: 90 mAh $g^{-1}$ at 2 A $g^{-1}$, GA-PDA: 178 mAh $g^{-1}$ at 2 A $g^{-1}$), and outstanding cycle stability (TTD-PDA: 298% capacity retention at 5 A $g^{-1}$ after 5,000 cycles, TTD-EDA: 3050% capacity retention at 5 A $g^{-1}$ after 5,000 cycles, GA-PDA: 892% capacity retention at 5 A $g^{-1}$ after 5,000 cycles). Combined with these results, the three organic Schiff-base polymers have been effectively verified as potential anode materials for LIBs. It is worth mentioning that the vast majority of traditional organic electrode materials are designed as conjugated structures, which greatly limits the flexibility of organic materials. Our results indicate that nonconjugated organic polymers are also highly promising anode materials for LIBs, greatly expanding the design scheme of organic electrodes.

## ■ ASSOCIATED CONTENT

### Supporting Information

The Supporting Information is available free of charge at https://pubs.acs.org/doi/10.1021/acsomega.3c09299.

> Rate performance of CNT, cyclic stability of CNT and individual Schiff-bases, apparent rate performance and cyclic stability of the Schiff-bases, calculation method for the actual specific capacity, and Warburg factors and the diffusion coefficient of $Li^+$ (PDF)

## ■ AUTHOR INFORMATION


### Corresponding Authors

**Xiaoyue Mu** − *State Key Laboratory of Supramolecular Structure and Materials, College of Chemistry, Jilin University, Changchun 130012, P. R. China*; Email: xymu@jlu.edu.cn

**Ying Mu** − *State Key Laboratory of Supramolecular Structure and Materials, College of Chemistry, Jilin University, Changchun 130012, P. R. China*; orcid.org/0000-0002-7084-1791; Email: ymu@jlu.edu.cn

### Author

**Jinkai Zhang** − *State Key Laboratory of Supramolecular Structure and Materials, College of Chemistry, Jilin University, Changchun 130012, P. R. China*

Complete contact information is available at: https://pubs.acs.org/10.1021/acsomega.3c09299


### Author Contributions

J.Z., X.M., and Y.M. conceived the idea and designed the experiments. J.Z. performed the experiments. J.Z., X.M., and Y.M. cowrote the manuscript, performed the data analyses and participated in the discussions. X.M. and Y.M. directed the project.

### Notes

The authors declare no competing financial interest.

## ■ ACKNOWLEDGMENTS

We are grateful for the financial support from the National Natural Science Foundation of China (51673078).

## ■ REFERENCES


(1) Kannan, N.; Vakeesan, D. Solar energy for future world: - A review. *Renew. Sust. Energy Rev.* **2016**, *62*, 1092−1105.

(2) Palacín, M. R. Recent advances in rechargeable battery materials: a chemist's perspective. *Chem. Soc. Rev.* **2009**, *38*, 2565−2575.

(3) Deng, D. Li−ion batteries: basics, progress, and challenges. *Energy Sci. Eng.* **2015**, *3*, 385−418.

(4) Wu, M.; Cui, Y.; Bhargav, A.; Losovyj, Y.; Siegel, A.; Agarwal, M.; Ma, Y.; Fu, Y. Z. Organotrisulfide: A High Capacity Cathode Material for Rechargeable Lithium Batteries. *Angew. Chem., Int. Ed.* **2016**, *55*, 10027−10031.

(5) Adam, T. J.; Liao, G.; Petersen, J.; Geier, S.; Finke, B.; Wierach, P.; Kwade, A.; Wiedemann, M. Multifunctional Composites for Future Energy Storage in Aerospace Structures. *Energies* **2018**, *11*, 335.

(6) Capovilla, G.; Cestino, E.; Reyneri, L. M.; Romeo, G. Modular Multifunctional Composite Structure for Cubesat Applications: Preliminary Design and Structural Analysis. *Aerospace* **2020**, *7*, 17.

(7) Bruce, P. G.; Scrosati, B.; Tarascon, J. M. Nanomaterials for Rechargeable Lithium Batteries. *Angew. Chem., Int. Ed.* **2008**, *47*, 2930−2946.

(8) Jin, J.; Wu, L.; Huang, S.; Yan, M.; Wang, H.; Chen, L.; Hasan, T.; Li, Y.; Su, B. L. Hierarchy Design in Metal Oxides as Anodes for Advanced Lithium-ion Batteries. *Small Methods* **2018**, *2*, 1800171.

(9) Roy, P.; Srivastava, S. K. Nanostructured anode materials for lithium ion batteries. *J. Mater. Chem. A* **2015**, *3*, 2454−2484.

(10) Rajkamal, A.; Thapa, R. Carbon Allotropes as Anode Material for Lithium-Ion Batteries. *Adv. Mater. Technol.* **2019**, *4*, 1900307.

(11) Wang, H. G.; Yuan, S.; Ma, D. L.; Huang, X. L.; Meng, F. L.; Zhang, X. B. Tailored Aromatic Carbonyl Derivative Polyimides for High-Power and Long-Cycle Sodium-Organic Batteries. *Adv. Energy Mater.* **2014**, *4*, 1301651.

(12) Song, C. K.; Eckstein, B. J.; Tam, T. L. D.; Trahey, L.; Marks, T. J. Conjugated Polymer Energy Level Shifts in Lithium−Ion Battery Electrolytes. *ACS Appl. Mater. Interfaces.* **2014**, *6*, 19347−19354.

(13) Wu, H.; Yu, G.; Pan, L.; Liu, N.; McDowell, M. T.; Bao, Z.; Cui, Y. Stable Li-ion battery anodes by *in-situ* polymerization of conducting hydrogel to conformally coat silicon nanoparticles. *Nat. Commun.* **2013**, *4*, 1943−1948.

(14) Ma, T.; Zhao, Q.; Wang, J. B.; Pan, Z.; Chen, J. A Sulfur Heterocyclic Quinone Cathode and a Multifunctional Binder for a High-Performance Rechargeable Lithium-Ion Battery. *Angew. Chem., Int. Ed.* **2016**, *55*, 6428−6432.

(15) Wang, Y.; Liu, Z.; Liu, H.; Liu, H.; Li, B.; Guan, S. A Novel High-Capacity Anode Material Derived from Aromatic Imides for Lithium-Ion Batteries. *Small* **2018**, *14*, 1704094.

(16) Ahmad, A.; Meng, Q. H.; Melhi, S.; Mao, L. J.; Zhang, M.; Han, B. H.; Lu, K.; Wei, Z. X. A Hierarchically Porous Hypercrosslinked and Novel Quinone based Stable Organic Polymer Electrode for Lithium-Ion Batteries. *Electrochim. Acta* **2017**, *255*, 145−152.

(17) Ke, H. Z.; Zhang, Q. H.; Zhang, X. M.; Cheng, G.; Sun, Y. B.; Li, J.; Cheng, H. S. Hydroquinone-based conjugated Schiff base polymer as anode material for lithium ion batteries. *Mater. Lett.* **2021**, *286*, No. 129235.

(18) Liu, Z. M.; Li, H. F.; He, Y.; Sun, H. R.; Xu, C. M.; Li, H. C.; Wang, X. J.; Zhang, G. X.; Sun, Z. H.; Wei, Q.; Song, T.; Paik, U. An integrated strategy based on Schiff base reactions to construct unique two-dimensional nanostructures for intrinsic pseudocapacitive sodium/lithium storage. *Chem. Eng. J.* **2022**, *429*, No. 132339.

(19) Zhang, Z.; Zhou, Y. F.; Chen, P. P.; Zeng, S. H.; Nie, W. Y.; Xu, Y. Investigation of Capacity Increase in Schiff-Base Networks as the Organic Anode for Lithium-Ion Batteries. *ACS Appl. Energy. Mater.* **2021**, *4*, 12882−12891.
(20) Sun, Y. B.; Sun, Y. H.; Pan, Q. Y.; Li, G.; Han, B.; Zeng, D. L.; Zhang, Y. F.; Cheng, H. S. A hyperbranched conjugated Schiff base polymer network: a potential negative electrode for flexible thin film batteries. *Chem. Commun.* **2016**, *52*, 3000−3002.
(21) Zhai, L.; Li, G.; Yang, X.; Park, S.; Han, D.; Mi, L.; Wang, Y.; Li, Z.; Lee, S. Y. 30 $Li^+$-Accommodating Covalent Organic Frameworks as Ultralong Cyclable High-Capacity Li-Ion Battery Electrodes. *Adv. Funct. Mater.* **2022**, *32*, 2108798.
(22) Li, Z. H.; Ji, W. Y.; Wang, T. X.; Ding, X. S.; Han, B. H.; Feng, W. Maximized lithiophilic carbonyl units in covalent organic frameworks as effective Li ion regulators for lithium metal batteries. *Chem. Eng. J.* **2022**, *437*, No. 135293.
(23) Man, Z. M.; Li, P.; Zhou, D.; Zang, R.; Wang, S. J.; Li, P. X.; Liu, S. S.; Li, X. M.; Wu, Y. H.; Liang, X. H.; Wang, G. X. High-performance lithium−organic batteries by achieving 16 lithium storage in poly(imine-anthraquinone) J. *Mater. Chem. A* **2019**, *7*, 2368−2375.
(24) Kang, H. W.; Liu, H. L.; Li, C. X.; Sun, L.; Zhang, C. F.; Gao, H. C.; Yin, J.; Yang, B. C.; You, Y.; Jiang, K. C.; Long, H. J.; Xin, S. Polyanthraquinone-Triazine—A Promising Anode Material for High-Energy Lithium-Ion Batteries. *ACS Appl. Mater. Interfaces* **2018**, *10*, 37023−37030.
(25) Wu, J.; Rui, X.; Wang, C.; Pei, W. B.; Lau, R.; Yan, Q.; Zhang, Q. Nanostructured Conjugated Ladder Polymers for Stable and Fast Lithium Storage Anodes with High-Capacity. *Adv. Energy Mater.* **2015**, *5*, 1402189.
(26) Renault, S.; Oltean, V. A.; Araujo, C. M.; Grigoriev, A.; Edström, K.; Brandell, D. Superlithiation of Organic Electrode Materials: The Case of Dilithium Benzenedipropiolate. *Chem. Mater.* **2016**, *28*, 1920−1926.
(27) Zhang, Z. W.; Li, Z. Q.; Hao, F. B.; Wang, X. K.; Li, Q.; Qi, Y. X.; Fan, R. H.; Yin, L. W. 3D Interconnected Porous Carbon Aerogels as Sulfur Immobilizers for Sulfur Impregnation for Lithium-Sulfur Batteries with High Rate Capability and Cycling Stability. *Adv. Funct. Mater.* **2014**, *24*, 2500−2509.
(28) Zhao, G. F.; Zhang, Y. H.; Gao, Z. H.; Li, H. N.; Liu, S. M.; Cai, S.; Yang, X. F.; Guo, H.; Sun, X. L. Dual Active Site of the Azo and Carbonyl-Modified Covalent Organic Framework for High-Performance Li Storage. *ACS Energy Lett.* **2020**, *5*, 1022−1031.
(29) Yang, X. B.; Lin, C.; Han, D. D.; Li, G. J.; Huang, C.; Liu, J.; Wu, X. L.; Zhai, L. P.; Mi, L. W. In situ construction of redox−active covalent organic frameworks/carbon nanotube composites as anodes for lithium−ion batteries. *J. Mater. Chem. A* **2022**, *10*, 3989−3995.
(30) Schon, T. B.; Tilley, A. J.; Kynaston, E. L.; Seferos, D. S. Three-Dimensional Arylene Diimide Frameworks for Highly Stable Lithium Ion Batteries. *ACS Appl. Mater. Interfaces* **2017**, *9*, 15631−15637.
(31) Han, X. Y.; Qing, G. Y.; Sun, J. T.; Sun, T. L. How Many Lithium Ions Can Be Inserted onto Fused $C_6$ Aromatic Ring Systems? *Angew. Chem.* **2012**, *124*, 5237−5241.
(32) Lei, Z.; Chen, X.; Sun, W.; Zhang, Y.; Wang, Y. Exfoliated Triazine-Based Covalent Organic Nanosheets with Multielectron Redox for High-Performance Lithium Organic Batteries. *Adv. Energy Mater.* **2019**, *9*, 1801010.
(33) Wang, P.; Yang, F. S.; Li, L.; Cai, Z. S. Flame retardancy and mechanical properties of epoxy thermosets modified with a novel DOPO-based oligomer. *Polym. Degrad. Stab.* **2016**, *129*, 156−167.
(34) Huang, L.; Mo, C.; Qu, A.; Chen, Y. The effects of terminal groups on the structure and photocatalytic performance of imine-linked conjugated polymers. *J. Photochem. Photobiol., A* **2023**, *438*, No. 114481.
(35) Gao, C. Y.; Chen, G. M. A new strategy to construct thermoelectric composites of SWCNTs and poly-Schiff bases with 1,4-diazabuta-1,3-diene structures acting as bidentate-chelating units. *J. Mater. Chem. A* **2016**, *4*, 11299−11306.
(36) Wang, J. C.; Senkovska, I.; Oschatz, M.; Lohe, M. R.; Borchardt, L.; Heerwig, A.; Liu, Q.; Kaskel, S. Imine-Linked Polymer-Derived Nitrogen-Doped Microporous Carbons with Excellent $CO_2$ Capture Properties. *ACS Appl. Mater. Interfaces* **2013**, *5*, 3160−3167.
(37) Lei, Z.; Yang, Q.; Xu, Y.; Guo, S.; Sun, W.; Liu, H.; Lv, L. P.; Zhang, Y.; Wang, Y. Boosting lithium storage in covalent organic framework via activation of 14-electron redox chemistry. *Nat. Commun.* **2018**, *9*, 576−588.
(38) Wu, J. S.; Rui, X. H.; Long, G. K.; Chen, W. Q.; Yan, Q. Y.; Zhang, Q. C. Pushing Up Lithium Storage Through Nanostructured Polyazaacene Analogues as Anode. *Angew. Chem., Int. Ed.* **2015**, *54*, 7354−7358.
(39) Wang, J.; Yao, H. Y.; Du, C. Y.; Guan, S. W. Polyimide schiff base as a high-performance anode material for lithium-ion batteries. *J. Power Sources.* **2021**, *482*, No. 228931.
(40) Zhang, J. K.; Mu, Y. A Schiff based *p*-phenylenediimine polymer as high capacity anode materials for stable lithium ion batteries. *Electrochim. Acta* **2023**, *450*, No. 142276.
(41) Buyukcakir, O.; Ryu, J.; Joo, S. H.; Kang, J.; Yuksel, R.; Lee, J.; Jiang, Y.; Choi, S.; Lee, S. H.; Kwak, S. K.; Park, S.; Ruoff, R. S. Lithium Accommodation in a Redox-Active Covalent Triazine Framework for High Areal Capacity and Fast-Charging Lithium-Ion Batteries. *Adv. Funct. Mater.* **2020**, *30*, 2003761−2003771.


https://doi.org/10.1021/acsomega.3c09299
*ACS Omega* 2024, 9, 12967−12975